P2.5 VARIATIOANL RETRIEVAL OF RAINDROP SIZE DISTRIBUTION FROM POLARIMETRIC RADAR DATA IN PRESENCE OF ATTENUATION

Qing Cao[1,3], Guifu Zhang[2,3] and Ming Xue[2,4]

1: School of Electrical and Computer Engineering, University of Oklahoma, Norman, OK 73072

2: School of Meteorology, University of Oklahoma, Norman, OK 73072

3: Atmospheric Radar Research Center, University of Oklahoma, Norman, OK 73072

4: Center for Analysis and Prediction of Storms, University of Oklahoma, Norman, OK 73072

1. INTRODUCTION

Most national weather radar networks in the world operate at the C-band. The WSR-88D radar network in the United States works at the S-band frequency (or 10 cm wavelength) but many weather radars in other countries as well as the TDWR (Terminal Doppler Weather Radars) of the U.S. operate at the C-band (5 cm wavelength). Recently, X-band (3 cm wavelength) weather radars such as those in the CASA (Center for Collaborative Adaptive Sensing of the Atmosphere) IP1 network have received more attention. Unlike S-band radars, the propagation effect of precipitation attenuation on C-band and X-band measurements cannot be ignored. Attenuation correction is significant problem for radar-based rain estimation and precipitation microphysics studies at these shorter wavelengths.

For single-polarization radars, attenuation correction is mainly based on the Hitschfeld-Bordan (H-B) method and its revised versions (e.g., Delrieu et al. 2000; Zhang et al. 2004; Berne and Uijlenhoet 2006). With dual-polarization radars, the measured propagation phases (e.g., differential phase or specific differential phase) have been widely used for attenuation correction. Such algorithms include direct phase correction (DP) method (e.g., Bringi et al. 1990), data fitting method (Ryzhkov and Zrnic 1995), ZPHI algorithm (Testud et al. 2000), self-consistence (SC) method (Bringi et al. 2001) and revised SC methods (e.g., Park et al. 2005; Vulpiani et al. 2005; Gorgucci and Baldini 2007; Liu et al. 2006; Ryzhkov et al. 2007). All these algorithms apply various empirical relations associated with the attenuation. For example, the deterministic power law relation between the attenuation and radar reflectivity is the basis for the H-B and revised H-B algorithms. The power law relations between the attenuation and specific differential phase (K_{DP}) are essential for phase-based attenuation corrections. These empirical relations should be uniquely known for the DP method while the coefficients could be adjusted by the SC method and its revised versions.

There are problems in the algorithms of attenuation correction mentioned above. The attenuation estimated from empirical relations may have been affected by the strong constraints that sacrifice a lot of physical variability. On the other hand, the measurement error, which can further deteriorate the attenuation estimation, has not been fully taken into account in these algorithms. There are possible ways to solve these problems. Since drop size distribution (DSD) of precipitating hydrometeors is fundamental for precipitation microphysics and radar measurements, the sacrifice of physical variability can be mitigated by estimating DSD parameters, which are used to estimate the attenuation (e.g., Meneghini and Liao 2007). In addition, the effect of measurement error can be minimized through a variational approach by optimizing the use of all available measurements with error-based weights (e.g., Hogan 2007). The combination of these two approaches should have great potential to improve attenuation correction and QPE. To do the above, the DSD parameters will need to be estimated as part of the

* Corresponding author address: Qing Cao; 120 David L. Boren Blvd. Suite 5900, Norman, OK 73072, U.S.A.; E-mail: qingcao@ou.edu

state vector. Because of the involvement of the DSD parameters in the observation operator, the variational scheme becomes highly non-linear. The forward model of radar measurements (i.e., attenuated observations) and the corresponding partial derivatives are complicated functions of the DSD parameters. The development of adjoint codes is a problem.

In this study, two approaches mentioned above are combined for the first time to correct attenuation and estimate rain DSD parameters from the X-band polarimetric radar data (PRD). The DSD is retrieved through a two-dimensional variational scheme. Attenuation effect is built into the forward observation operator and the attenuation correction is accomplished adaptively during the iterative optimization/estimation process. The rest of the paper is organized as follows. The methodology is described in the section 2. The algorithm is evaluated in section 3 using simulated X-band PRD from measured S-band PRD. The retrieval based on real X-band PRD is analyzed in section 4. Possible error sources of the algorithm are discussed in section 5 and conclusions in section 6.

2. METHODOLOGY

2.1 Variational approach

The PRD used for the variational retrieval are radar reflectivity of horizontal polarization (Z_H), differential reflectivity (Z_{DR}), and K_{DP}. The optimal use of the measurements involves the minimization of cost function ,

$$J(\mathbf{x}) = J_b(\mathbf{x}) + \mathbf{w}_{Z_H} J_{Z_H}(\mathbf{x}) + \mathbf{w}_{Z_{DR}} J_{Z_{DR}}(\mathbf{x}) + \mathbf{w}_{K_{DP}} J_{K_{DP}}(\mathbf{x}) \quad (1)$$

where,

$$J_b(\mathbf{x}) = \frac{1}{2}(\mathbf{x}-\mathbf{x}_b)^{\mathrm{T}} \mathbf{B}^{-1}(\mathbf{x}-\mathbf{x}_b), \quad (2a)$$

$$J_{Z_H}(\mathbf{x}) = \frac{1}{2}\left[H_{Z_H}(\mathbf{x}) - \mathbf{y}_{Z_H}\right]^{\mathrm{T}} \mathbf{R}_{Z_H}^{-1}\left[H_{Z_H}(\mathbf{x}) - \mathbf{y}_{Z_H}\right], \quad (2b)$$

$$J_{Z_{DR}}(\mathbf{x}) = \frac{1}{2}\left[H_{Z_{DR}}(\mathbf{x}) - \mathbf{y}_{Z_{DR}}\right]^{\mathrm{T}} \mathbf{R}_{Z_{DR}}^{-1}\left[H_{Z_{DR}}(\mathbf{x}) - \mathbf{y}_{Z_{DR}}\right], \quad (2c)$$

$$J_{K_{DP}}(\mathbf{x}) = \frac{1}{2}\left[H_{K_{DP}}(\mathbf{x}) - \mathbf{y}_{K_{DP}}\right]^{\mathrm{T}} \mathbf{R}_{K_{DP}}^{-1}\left[H_{K_{DP}}(\mathbf{x}) - \mathbf{y}_{K_{DP}}\right] \quad (2d)$$

The cost function J is composed of four parts. J_b is the background part. The other three terms correspond to the observations of Z_H, Z_{DR}, and K_{DP}, respectively. Superscript T denotes matrix transpose. $\mathbf{w}$ represents relative weights of the observation terms, which is associated with the signal-to-noise ratio (SNR). $\mathbf{x}$ is the state vector and $\mathbf{x}_b$ is the background or first guess. $\mathbf{y}$ contains the radar observations. H denotes the nonlinear observation operator of radar variables. $\mathbf{B}$ is the background error covariance matrix. $\mathbf{R}$ is the observational error covariance matrix. The $\mathbf{w}$ can be regarded as a part of $\mathbf{R}$. In this study, we separate them for the convenience of defining a simple $\mathbf{w}$ in term of SNR. Subscripts Z_H, Z_{DR} and K_{DP} are used to denote the terms for corresponding the observations. In the above equations, we try to follow the standard notations used in modern data assimilation literature, as defined in Ide et al. (1997).

The size of matrix $\mathbf{B}$ is n^2 where n is the size of state vector $\mathbf{x}$. The full matrix is usually huge. Matrix computation and storage, especially for the inversion of $\mathbf{B}$, can be a major problem during the iterative minimization of the cost function. To solve this problem, a new state variable $\mathbf{v}$ is introduced, written as,

$$\mathbf{v} = \mathbf{D}^{-1}\delta\mathbf{x}, \quad (3)$$

with $\delta\mathbf{x} = \mathbf{x} - \mathbf{x}_b$ and $\mathbf{D}\mathbf{D}^{\mathrm{T}} = \mathbf{B}$ (Parrish and Derber 1992). δ is the notation of the increment. $\mathbf{D}$ is the square root of the background error covariance matrix $\mathbf{B}$. The cost function is then rewritten as,

$$J(\mathbf{v}) = \frac{1}{2}\mathbf{v}^{\mathrm{T}}\mathbf{v} + \frac{1}{2}\mathbf{w}_{Z_H}\left[H_{Z_H}(\mathbf{x}_b + \mathbf{D}\mathbf{v}) - \mathbf{y}_{Z_H}\right]^{\mathrm{T}} \mathbf{R}_{Z_H}^{-1}\left[H_{Z_H}(\mathbf{x}_b + \mathbf{D}\mathbf{v}) - \mathbf{y}_{Z_H}\right] +$$

$$\frac{1}{2}\mathbf{w}_{Z_{DR}}\left[H_{Z_{DR}}(\mathbf{x}_b+\mathbf{Dv})-\mathbf{y}_{Z_{DR}}\right]^{\mathrm{T}}\mathbf{R}_{Z_{DR}}^{-1}\left[H_{Z_{DR}}(\mathbf{x}_b+\mathbf{Dv})-\mathbf{y}_{Z_{DR}}\right]+$$

$$\frac{1}{2}\mathbf{w}_{K_{DP}}\left[H_{K_{DP}}(\mathbf{x}_b+\mathbf{Dv})-\mathbf{y}_{K_{DP}}\right]^{\mathrm{T}}\mathbf{R}_{K_{DP}}^{-1}\left[H_{K_{DP}}(\mathbf{x}_b+\mathbf{Dv})-\mathbf{y}_{K_{DP}}\right] \quad (4)$$

In this way, the inversion of B is avoided. The minimization of cost function J is achieved by searching the minimum gradient of cost function $\nabla_{\mathbf{v}}J$, which is given by,

$$\begin{aligned}\nabla_{\mathbf{v}}J=\mathbf{v}&+\mathbf{w}_{Z_H}\mathbf{D}^{\mathrm{T}}\mathbf{H}_{Z_H}^{\mathrm{T}}\mathbf{R}_{Z_H}^{-1}\left(\mathbf{H}_{Z_H}^{\mathrm{T}}\mathbf{Dv}-\mathbf{d}_{Z_H}\right)\\&+\mathbf{w}_{Z_{DR}}\mathbf{D}^{\mathrm{T}}\mathbf{H}_{Z_{DR}}^{\mathrm{T}}\mathbf{R}_{Z_{DR}}^{-1}\left(\mathbf{H}_{Z_{DR}}^{\mathrm{T}}\mathbf{Dv}-\mathbf{d}_{Z_{DR}}\right)\\&+\mathbf{w}_{K_{DP}}\mathbf{D}^{\mathrm{T}}\mathbf{H}_{K_{DP}}^{\mathrm{T}}\mathbf{R}_{K_{DP}}^{-1}\left(\mathbf{H}_{K_{DP}}^{\mathrm{T}}\mathbf{Dv}-\mathbf{d}_{K_{DP}}\right)\end{aligned} \quad (5)$$

H represents the Jacobian operator, a matrix containing the partial derivative of observation operator H with respective to each element of the state vector. **d** is the innovation vector of the observation, i.e., $\mathbf{d}=\mathbf{y}-H(\mathbf{x}_b)$.

The spatial influence of the observation is determined by the background error covariance matrix **B**. Huang (2000) showed that the element b_{ij} of matrix **B** could be modeled as a spatial filter,

$$b_{ij}=\sigma_b^2\exp\left[-\frac{1}{2}\left(\frac{r_{ij}}{r_L}\right)^2\right], \quad (6)$$

where subscripts i, j denotes two grid points in the analysis space. σ_b^2 is the background error covariance. r_{ij} indicates the distance between the i^{th} and j^{th} grid points. r_L is the decorrelation length of observed physical quantity. In this study, r_L is assumed to be constant in the two-dimensional analysis space, i.e., the error covariance is spatially homogeneous at horizontal plane, as is for the isotropic covariance option in Liu and Xue (2006). The square root of **B**, **D**, can be computed by applying a recursive filter described by Gao et al. (2004) and Liu et al. (2007). In this way, the cost of computation and storage can be reduced significantly (by a factor of **B** dimension), compared to the computation of inversion of **B**.

2.2 Forward observation operator

In this study, the state variables to be retrieved or estimated variationally are parameters in the assumed DSD model for the hydrometeors. The gamma distribution

$$N(D)=N_0D^{\mu}\exp(-\Lambda D) \quad (7)$$

is common used to model DSDs, where N_0 is a number concentration parameter is, μ is the shape parameter and Λ the slope parameter of the gamma DSD. In this study, we apply the gamma DSD model with a constraining relation derived by Cao et al. (2008),

$$\mu=-0.0201\Lambda^2+0.902\Lambda-1.718. \quad (8)$$

This relation is an update of constraint-gamma (C-G) DSD model proposed by Zhang et al. (2001) and it reduces the number of free parameters from 3 to 2. The C-G DSD model has been successfully used in direct DSD retrievals from radar measured Z_{H} and Z_{DR} (e.g., Brandes et al. 2004; Cao et al. 2008). It should be appropriate for testing our variational retrieval here. In our formulation, $N_0^*=\log_{10}(N_0)$ and Λ are chosen as the two state variables, thus the state vector **x** is composed of N_0^* and Λ at all grid points.

Given the two DSD parameters at each grid point, the DSD can be determined. Therefore, rain properties, including intrinsic Z_H and Z_{DR}, as well as K_{DP} can be estimated as well. Forward operators of Z_H, Z_{DR} and K_{DP} we use are given by Zhang et al. (2001),

$$Z_{H,V}=\frac{4\lambda^4}{\pi^4|K_w|^2}\int_0^{\infty}\left|f_{a,b}(\pi)\right|^2N(D)dD \quad (\mathrm{mm^6m^{-3}}), \quad (9a)$$

$$Z_{DR}=\log_{10}\frac{Z_H}{Z_V}(\mathrm{dB}), \quad (9b)$$

and

$$K_{DP} = \frac{180\lambda}{\pi}\int_0^\infty \mathrm{Re}\left[f_a(0) - f_a(0)\right]N(D)dD \ \ (\mathrm{deg\ km^{-1}}) \tag{10}$$

where $f_a(\pi)$ and $f_b(\pi)$ represent the backscattering amplitudes at horizontal and vertical polarizations, respectively. Similarly, $f_a(0)$ and $f_b(0)$ represent forward scattering amplitudes. λ is the wavelength. $K_w = (\varepsilon_r - 1)/(\varepsilon_r + 2)$ and ε_r is the complex dielectric constant of water. Re( ) denotes the real part of a complex value. The scattering amplitudes $f_{a,b}(0/\pi)$ are calculated based on the T-matrix method. For computational efficiency, pre-calculated values of the scattering amplitudes are stored in a lookup table for raindrop diameters from 0.1 mm to 8.0 mm and they are used in the numerical integrations of the above equations

Specific attenuations at horizontal (A_H) and vertical (A_V) polarizations can be calculated by

$$A_{H,V} = 4.343\times 10^3 \int_0^\infty \sigma_{ext}^{H,V}(D)N(D)dD \ \ (\mathrm{dB\ km^{-1}}), \tag{11}$$

where $\sigma_{ext}^{H,V}$ is the extinction cross section at horizontal or vertical polarizations, respectively. The specific differential attenuation A_{DP} is defined as,

$$A_{DP} = A_H - A_V \ \ (\mathrm{dB\ km^{-1}})\ . \tag{12}$$

If specific attenuations are known, the attenuated Z_H and Z_{DR} at each range gate can be calculated by,

$$Z_H^a(n) = Z_H(n) - 2\sum_{i=1}^{n-1} A_H(i)\Delta r, \tag{13a}$$

and,
$$Z_{DR}^a(n) = Z_{DR}(n) - 2\sum_{i=1}^{n-1} A_{DP}(i)\Delta r \tag{13b}$$

where numbers i and n denote the i^{th} and n^{th} range gates from the radar location, respectively. Δr is the range resolution.

2.3 Lookup table method

In Eq. (5), it is expensive to directly compute the transpose of linearized operator **H**, which is the matrix of the partial derivative. In general, adjoint method is applied to compute $\mathbf{H^T}$ efficiently without storing the full matrix. In this study, the calculations of radar variables [in Eqs.(8)-(10)] are based on the pre-calculated values of scattering amplitudes. Without the approximation (e.g., using a empirical relation to model the scattering amplitudes), it is difficult to represent the derivatives functionally in terms of DSD parameters. In such a case, it is a problem to develop an adjoint for the calculation of $\mathbf{H^T}$. In order to solve this problem, the lookup table method is applied.

The values of partial derivative of each of the polarimetric measurement variables, i.e., Z_H, Z_{DR}, or K_{DP}, with respect to each of the two state variables, i.e., Λ or N^*_0, at each grid point, are needed. That is, there are total six tables of the derivative (i.e., $\frac{\partial Z_H}{\partial \Lambda}, \frac{\partial Z_{DR}}{\partial \Lambda}, \frac{\partial K_{DP}}{\partial \Lambda}, \frac{\partial Z_H}{\partial N_0^*}, \frac{\partial Z_{DR}}{\partial N_0^*}, \frac{\partial K_{DP}}{\partial N_0^*}$) for the observation operator H. In each lookup table, the derivative values are pre-calculated for parameter Λ varying from 0 to 50 and parameter N^*_0 varying from 0 to 10. To ensure the accuracy, the range of each parameter is discretized at an interval of 0.1. As the results, each of the lookup table has $nvar \times 501 \times 101$ elements, $nvar$ is the dimension of Λ and N^*_0. This way, the partial derivative value for the operator H is found from these tables for any given values of Λ and N^*_0. Interpolation can be performed for values between the lookup table values of Λ or N^*_0 to further improve the accuracy. Generally, the nearly values in the lookup tables are sufficiently accurate for the iterative minimization of cost function because the parameter ranges are wide. For state variables out of the table range, derivative value at the end of the range is assumed although in practice this rarely happens.

With the lookup tables, the derivative calculation cost can be saved. In the similar way, the calculations of intrinsic (i.e., non-attenuated) Z_H, Z_{DR}, K_{DP}, A_H, and A_{DP} are made efficient by the lookup table method as well,

given any two state parameters. As a result, the observational operator H is computed as the combination of different values found in various lookup tables, avoiding integral calculations in the forward model. Preliminary results in following sections have demonstrated that the lookup table is an efficient tool to deal with non-linear forward models of complicated functions.

2.4. Iteration procedure

The iteration procedure of minimizing the cost function is shown in Fig. 1. At the beginning of the program, necessary data files such as all lookup tables, the background, radar measured Z_H, Z_{DR}, K_{DP}, and signal-to-noise ratio (SNR) are loaded. In the mean time, initial parameters of the variational scheme are configured. Radar measurements are then preprocessed. Within the analysis region, only radar measurements with SNR > 1dB are used. Moreover, observational weights are set differently. The weight (i.e., element of matrix **w**) is set to 1 for SNR > 20dB, 1/2 for SNR > 10dB, 1/4 for SNR > 5 dB and 1/8 for SNR < 5dB, respectively.

With initial state vector (e.g., set **v**=0), intrinsic variables (i.e., Z_H, Z_{DR}, K_{DP}, A_H, and A_{DP}) are found for each grid point through lookup tables. Corresponding Jacobian matrices **H**s are constructed based on the lookup tables as well. After the interpolation from grid points to the observation points, attenuated Z_H and Z_{DR} are calculated according to Eq. (13). Calculated polarimetric variables, i.e., Z_H, Z_{DR} and K_{DP}, and measured PRD are used in Eq. (5) to calculate the gradient of cost function. The initial first guess is always assumed to be the background. During the minimization process, the state vector is updated at each loop until the iteration is converged. If the background contains no useful information (e.g., the constant background), the analysis field based on the first guess may not be satisfactory enough. In such a case, the analysis result is considered as a new first guess and used to repeat the minimization process. In general, several outer loops would give the satisfactory result, which has a relatively small cost function.

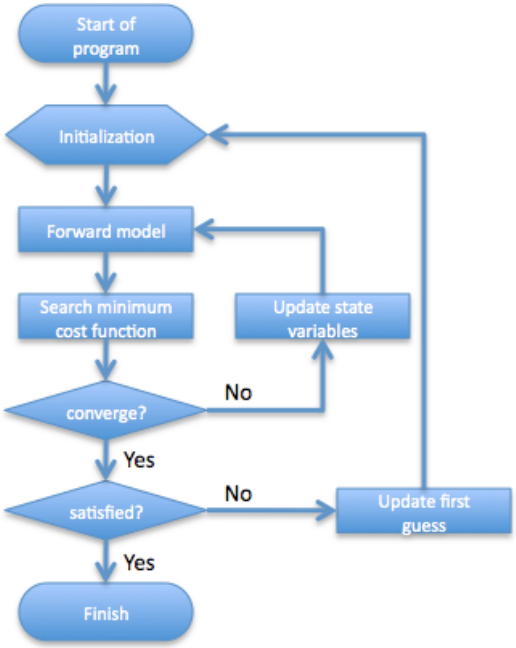

Fig. 1 Flowchart of variational retrieval scheme. Detailed description is given in section 2.4.

3. EVALUATION USING SIMULATED DATA

The advantage of using simulated data is that the truth is known and can be compared to the retrieved result. In this section, the variational approach is evaluated for X-band PRD simulated from real measurements of an S-band radar. The S-band measurements came from KOUN radar, an experimental polarimetric WSR-88D at Norman, Oklahoma. It is assumed that the simulated PRD are measured by two CASA IP1 radars (see, e.g., Xue et al. 2006), i.e., the radars located at Cyril (KCYR) and at Lawton (KLWE), Oklahoma, which are located at about 80 and 100 km southwest of the KOUN, respectively.

3.1 Simulation of X-band PRD

On May 8th, 2007, a convective system passed through Oklahoma from west to east. PPI images of Z_H and Z_{DR} as measured by KOUN at 0.5° elevation at 1230 UTC are shown in Fig. 2 and the data are used for the simulation. Two asterisks located at the southwest part of the image denote the locations of KLWE and KCYR. Two 20 km × 20 km regions indicated by the two square boxes in Fig. 2a are the analysis regions used to test our variational algorithm. It is worth noting that these two regions include a part of storm core, where the attenuation can be notable at X-band frequency.

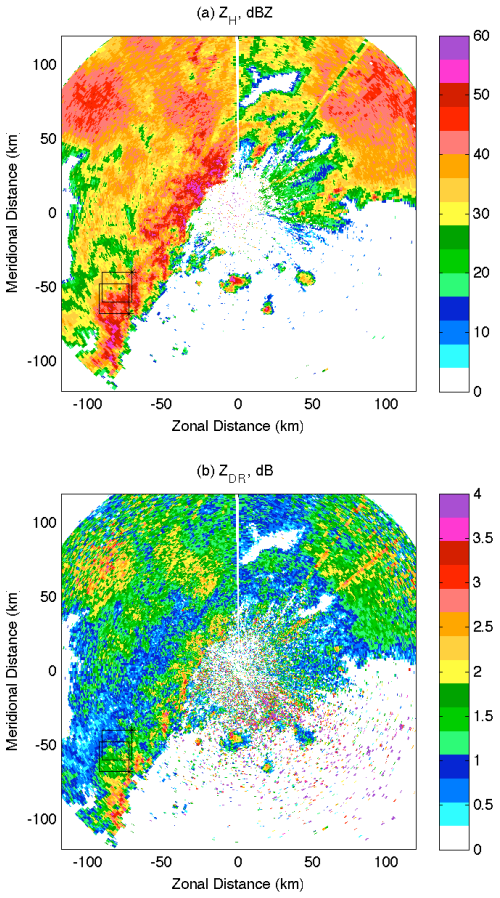

Fig. 2 (a) Z_H, (b) Z_{DR} measured by KOUN on the elevation angle of 0.5° at 1230 UTC on May 8th, 2007. Two asterisks southwest of the figure denote locations of KLWE (north asterisk) and KCYR (south asterisk), respectively. Two solid line boxes indicate the regions used for the simulation.

The simulation procedure is described as follows. Take the simulation of KCYR measurements for an example. Firstly, assume the KCYR makes full 360° azimuth scans at 1° increment. The maximum range is 30 km and the range resolution is 48 meters. Secondly, interpolate KOUN measurements at the lowest elevation to each radar range gate of KCYR, ignoring the effect of radar elevation differences. Thirdly, interpolated Z_H and Z_{DR} are used to retrieve the "true" DSD for each radar range gate, assuming the contribution completely comes from the rain. Next, intrinsic PRD (i.e., Z_H, Z_{DR}, K_{DP}, A_H, and A_{DP}) are calculated based on the "true" DSD. After intrinsic PRD are obtained for all range gates, attenuated PRD are then calculated along each beam path. Finally, random noises are added to the attenuated PRD to simulate measurement errors. Measurement errors are assumed to be Gaussian random noises with standard deviations of 2 dB for Z_H (dBZ), 0.2 dB for Z_{DR} (dB), and 0.1° km^{-1} for K_{DP} (° km^{-1}), respectively.

3.2 Retrieval without model error

In the third step of X-band PRD simulation, the "true" DSD is retrieved from two S-band PRD, Z_H and Z_{DR}. The retrieval follows the procedure described by Cao et al. (2008). It is worth noting that the "true" DSD is assumed to follow the C-G model, which is the same as the DSD model used in the variational retrieval. That is to say, when X-band PRD are simulated in this way, there is no DSD model error (but the DSD parameters are not known before hand) in the variational algorithm. In this subsection, we first examine the performance of the variational algorithm, using the perfect DSD model. The simulated attenuated observations contain measurement errors.

In order to do the variational analysis, some configurations have been set in the program as follows. The analysis region is a 20 km × 20 km square shown by the box in Fig. 2. It is covered by 251 × 251 analysis points at 80 meter intervals. The initial background is

set to constant values over the whole analysis domain (N^*_0 is 3 and Λ is 4). These rough guesses may be far from the truth. In the variational scheme, the decorrelation scale L is set to be 20 grids, i.e., 1.6 km, which is reasonable for the spatial property of a storm. Default observation errors are 2 dB for Z_H, 0.2 dB for Z_{DR}, and 0.1° km^{-1} for K_{DP}, the same as those of simulated observations. Since the background is constant, the background error is set as 2, which is rather large.

The first experiment is performed for radar KCYR. Simulated PRD and retrieved results are shown in Fig. 3. Three columns from left to right show the images of Z_H, Z_{DR}, and K_{DP}, respectively. Three rows indicate different properties of PRD. The third row denotes the "true" PRD, which are simulated with the C-G DSD model, i.e., without model error for the variational algorithm. The second row represents the simulated observations. The attenuations have been applied to the simulated observations. Measurement errors have been added to them as well. The first row shows analysis results using the variational algorithm. The input data of the variational algorithm are the simulated PRD shown in the second row.

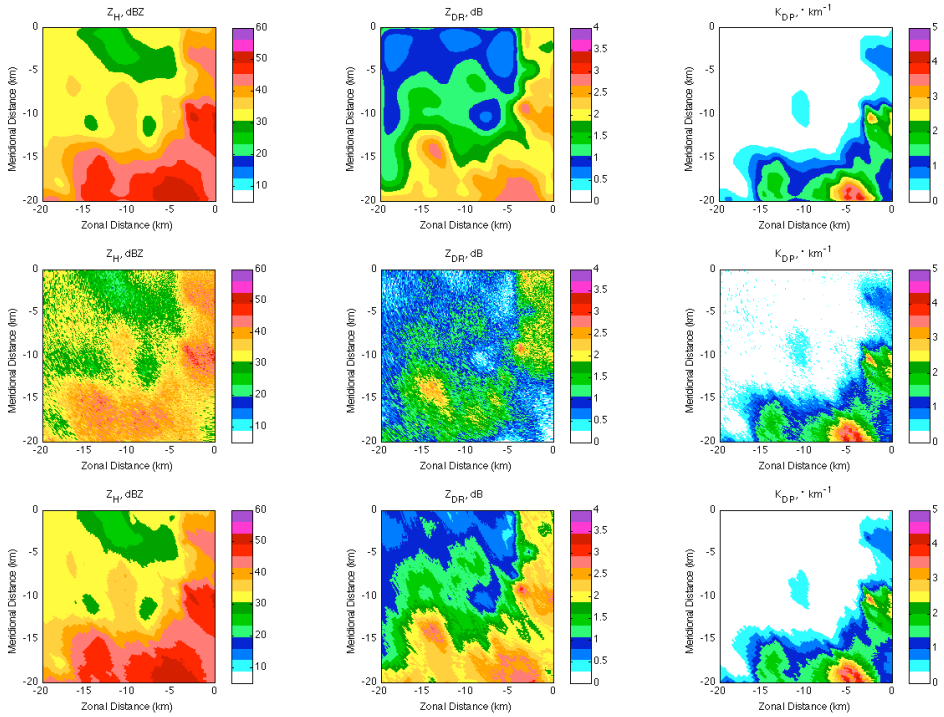

Fig. 3 Simulated PRD and retrieved results for KCYR. Three rows from top to bottom denote the retrieval results, the simulated PRD (with attenuation effect) and the truth fields, respectively. Three columns from left to right show the Z_H, Z_{DR}, and K_{DP}, respectively. True DSDs are assumed to follow C-G DSD model.

As Fig. 3 shows, the variational algorithm successfully retrieves Z_H, Z_{DR}, and K_{DP} even though observed PRD contain attenuations and noises. The analysis result match the truth very well except for some smoothing. The true PRD are interpolated onto the grid points and compared to the analysis results.

The biases of retrievals with respect to the true PRD are 0.11 dB, 0.01 dB and less than 0.001 ° km^{-1} for Z_H, Z_{DR}, and K_{DP}, respectively. Accordingly, the root-mean-square (rms) errors of retrievals are 0.47 dB, 0.10 dB and 0.06 ° km^{-1}. These results demonstrate the excellent performance of the variational algorithm in a perfect condition, i.e., with controlled measurement errors and without DSD model errors. Moreover, the lookup table method, as well as adaptive attenuation correction integrated in the forward model, has proven effective in this situation.

Similar analysis is performed for simulated PRD of KLWE. The results are shown in Fig. 4. In the analysis region, there are heavy rains around the radar so that the attenuation effect is more severe than the KCYR case shown in Fig. 3. This is obvious from the second row of Fig. 4. Simulated Z_H and Z_{DR} have very low values in the far distance. The strong attenuation close to the radar can negatively affect the minimization process of the cost function because the retrieval at far range is sensitive to the attenuation correction at near range. However, the variational algorithm still gave nearly perfect results. The biases of retrievals in Fig. 4 are 0.13 dB, 0.01 dB and 0.006 ° km^{-1}. The rms errors of retrievals are 0.40 dB, 0.09 dB and 0.07 ° km^{-1}. In the overlapping region of KCYR and KLWE radars, Fig. 3 and Fig. 4 show a good match for all three PRD.

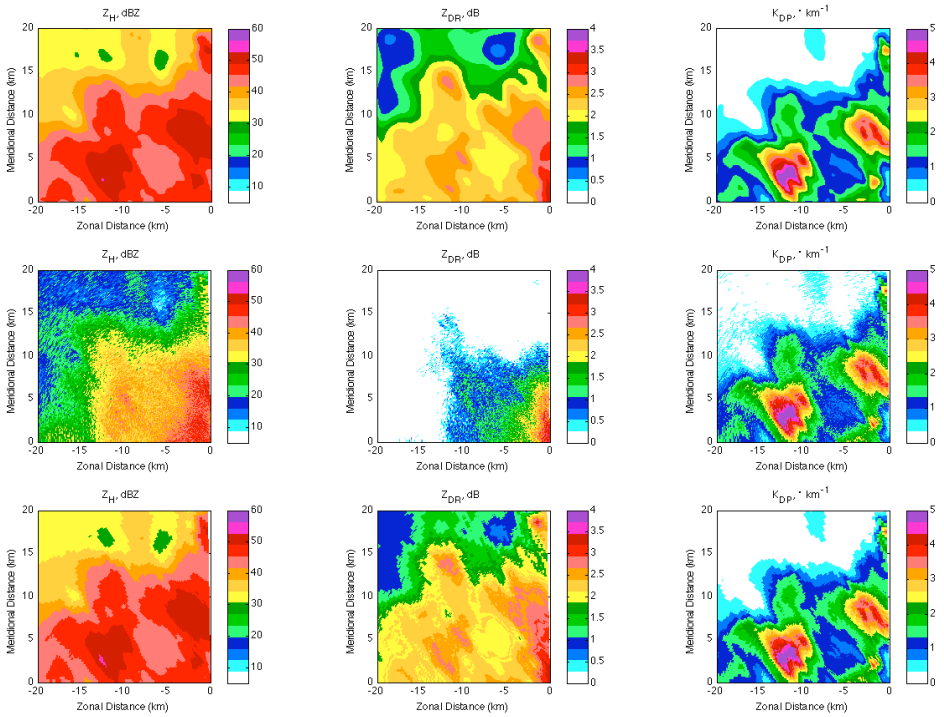

Fig. 4 The same as Fig. 3 but for KLWE

3.3. Retrieval with model error

In this section we test our variational retrieval procedure in the presence of DSD model error. During the simulation, the true DSD is assumed to follow the exponential model,

$$N(D) = N_0 \exp(-\Lambda D), \qquad (14)$$

instead of the C-G DSD model. There is an evident difference between C-G model and exponential model. The exponential model is equivalent to a gamma model with a shape parameter 0 while the C-G model is the gamma model with its shape parameter depending on the slope parameter. Since the variational algorithm applies the C-G model, simulated X-band PRD using exponential model can bring notable model error.

The simulation and retrieval procedures are similar to those described in previous subsection. We use the same S-band data so that the effect of model error can be perceived through the comparison. Corresponding results are shown in Fig. 5 for KCYR and in Fig. 6 for KLWE. Although the true PRD in Fig. 5 (or Fig. 6) do not have much difference with those in Fig. 3 (or Fig. 4), the intrinsic DSD are different.

It is seen that the retrieval results (first row) still match the truth (third row) very well even though DSD model error has been introduced. For Fig. 5, the biases of the retrievals are 0.09 dB, 0.01 dB, and 0.001°km^{-1} for Z_H, Z_{DR}, and K_{DP}, respectively. The rms errors of the retrievals are 0.46 dB, 0.10 dB and 0.06 ° km^{-1}. For Fig. 6, the corresponding biases are 0.16 dB, 0.03 dB, and 0.006 ° km^{-1}. The corresponding rms errors are 0.46 dB, 0.11 dB and 0.08 ° km^{-1}. Compared to the biases and rms errors in Figs. 3 and 4, there are no fundamental difference between them. That is to say, performance of the variational algorithm does not notably deteriorate with the inclusion of the DSD model error. The assumption of C-G DSD model is reasonable and practicable for this variational algorithm.

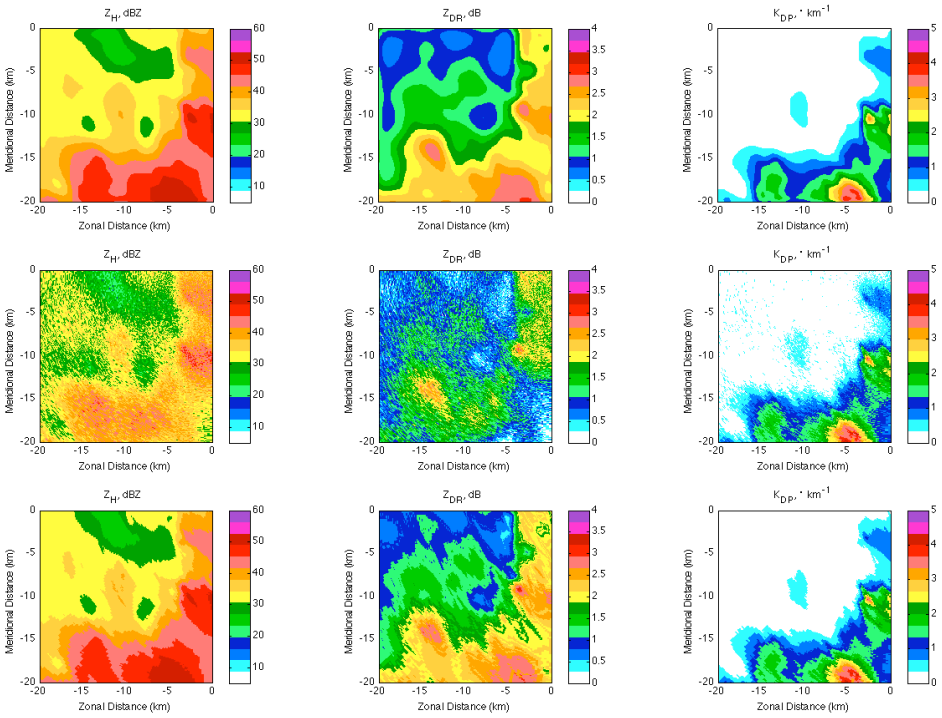

Fig. 5 The same as Fig. 3 but true DSDs are assumed to follow exponential DSD model

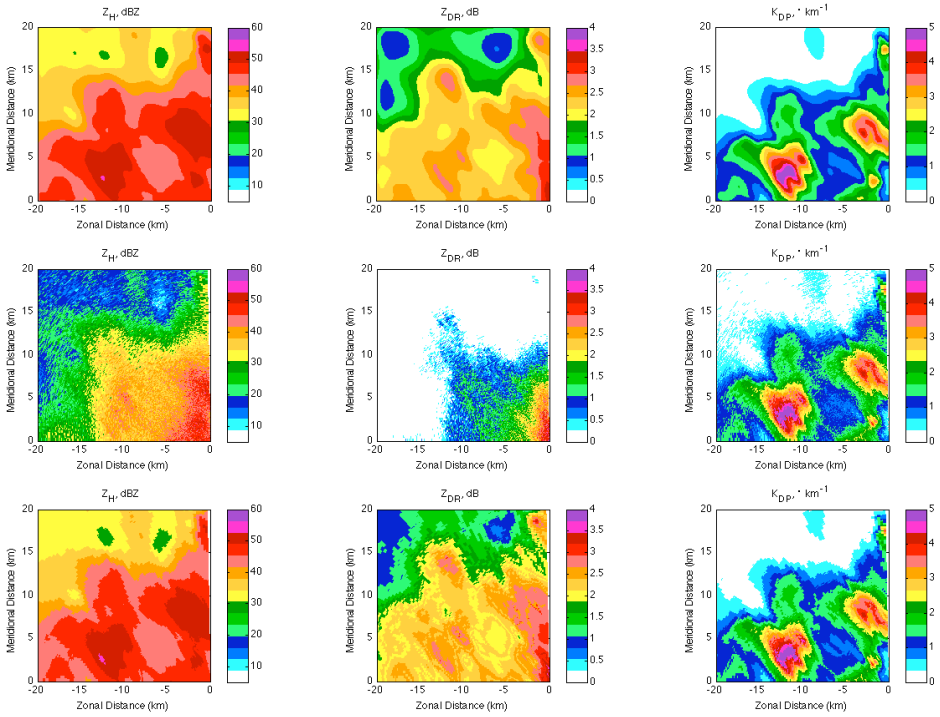

Fig. 6 The same as Fig. 5 but for KLWE

4. RETRIEVAL BASED ON REAL DATA

4.1 Real X-band data

The real data used for the retrieval test were collected by the same two CASA radars at an elevation angle of 2° at 1230 UTC on May 8, 2007. Figs. 7 and 8 show the PPI images of Z_H, Z_{DR}, K_{DP}, and SNR. The square boxes in the figures represent the analysis regions for the two radars. There are always some analysis regions, where the SNRs are less than 10 dB. The low SNR region is larger especially for the analysis region of KLWE (Fig. 8). Within the low SNR region, the data quality of PRD is problematic. In particular, K_{DP} is least reliable among three PRD. To mitigate the effect of poor data quality, some observational weighs have been introduced in the cost function [as shown in Eqs. (1) and (5) and described in section 2.4]. The default measurement errors are set to 2 dB for Z_H(dBZ), 0.4 dB for Z_{DR}(dB), and 0.2° km^{-1} for K_{DP} (° km^{-1}), respectively. The measurement errors for Z_{DR} and K_{DP} are twice of those assumed in the simulated data case because for real data Z_{DR} and K_{DP} usually have more uncertainty than Z_H. It can be obviously seen that real Z_H and Z_{DR} in Figs. 7 and 8 are much noisier than simulated Z_H and Z_{DR} in Figs. 3 and 4.

4.2 Constant background

The experiment in this subsection applies the same constant background as in the previous case (i.e., $N^*_0 =$ 3 and Λ = 4). The background error is set to 4. The retrieved results are shown in Figs. 9 and 10 for KCYR and KLWE, respectively.

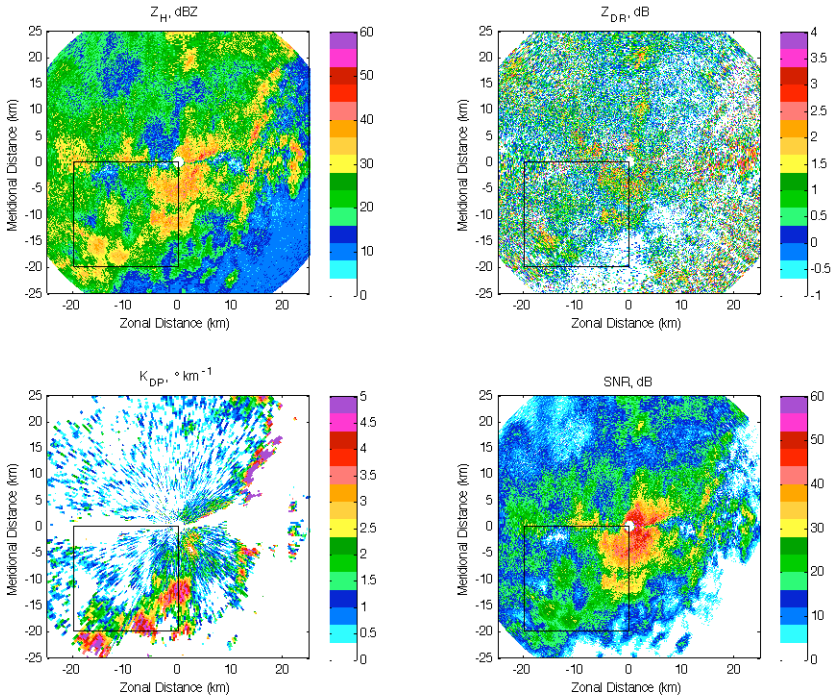

Fig. 7 (a) Z_H, (b) Z_{DR}, (c) K_{DP}, and (d) SNR as measured by KCYR at the elevation angle of 2° at 1230 UTC on May 8th, 2007. The square box region is the retrieval domain.

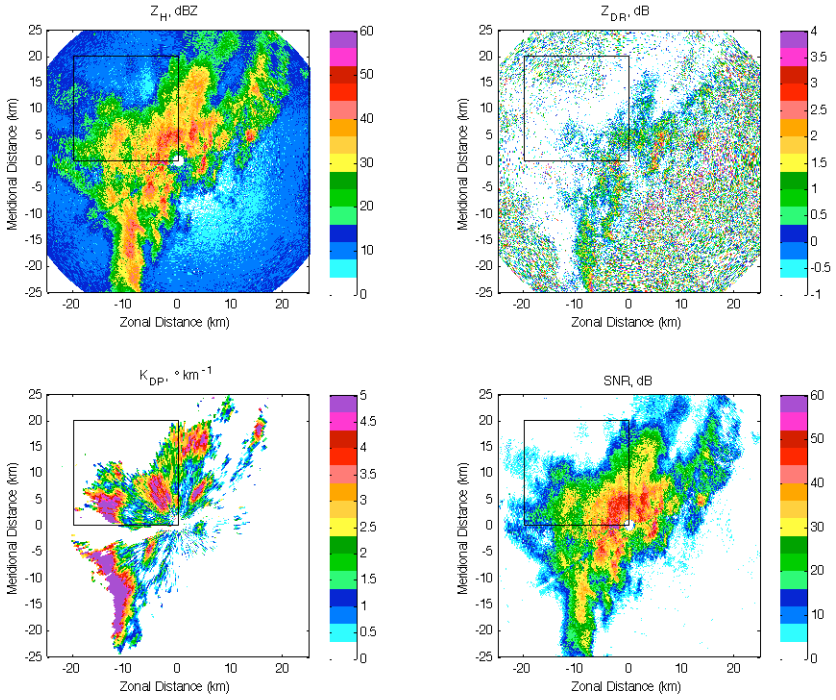

Fig. 8 The same as Fig. 7 but data were measured by KLWE.

It is known that polarimetric measurements at low SNR (e.g., SNR < 10 dB) are not reliable. Unfortunately, the constant background cannot provide any helpful information within the region of low SNR. Therefore, there exist great uncertainties during the retrieval. Moreover, since the attenuation correction process makes far range retrieval have a substantial dependence on the near range retrieval, the low SNR region could actually affect the retrieval almost at the entire region. This impact is evident in Figs. 9 and 10, especially for Z_{DR} and K_{DP}. The variational algorithm failed in this experiment when a constant background is assumed. It is reasonable to have such results because the variational retrieval is a global optimization system. If satisfactory retrieval were desired, good physical information (no matter from data or background) of the entire region should be provided. Otherwise, incorrect retrieval at one point might happen. Its negative effect could be spread through spatial correlation and incorrect attenuation correction, resulting in potential degradation of the entire system.

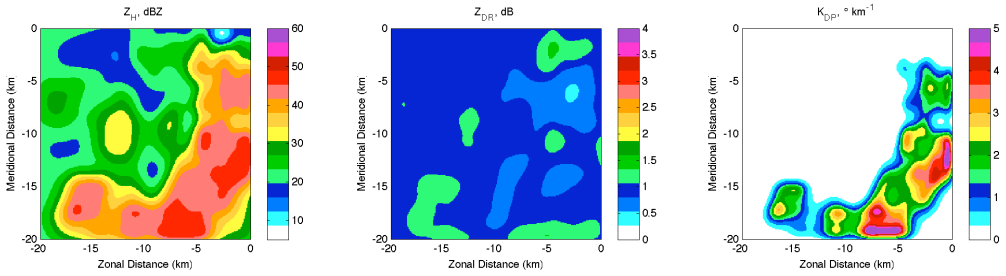

Fig. 9 Retrieved results based on KCYR radar measurements. The background was set to be constant. From left to right: (a) Z_H, (b) Z_{DR}, (c) K_{DP}.

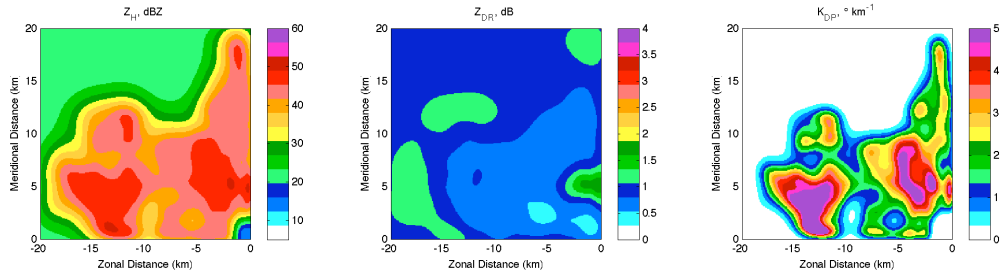

Fig. 10 The same as Fig. 9 but for the retrieval of KLWE radar measurements.

4.3 Background based on S-band measurements

The S-band radar measurements can be an additional source in providing useful information to compensate for the X-band radar measurements of bad data quality. The following experiment applies the same example as studied in the previous subsection except that the background is obtained from the S-band radar measurements. In section 2, we have applied KOUN measured Z_H and Z_{DR} to simulate a "truth" field (Figs. 3 and 4, the third row). Here we use the simulated "truth" field as the background. Generally, the S-band measurements should be close to the truth though there exist model error and measurement error effects. Consequently, using the retrieved DSD parameters as the background should have a smaller background error than using constant background. In this experiment the background error is set to 0.5, representing a moderate

error. For example, given the same Λ, N^*_0 error of 0.5 introduces 5 dB error for Z_H.

The variational retrieval results are shown in Figs. 11 and 12 for KCYR and KLWE, respectively. As expected, the background has compensated for the X-band data with low quality so that the performance of the variational algorithm was stable and satisfactory. Since we do not know the truth, the reasonableness can be examined by comparing the results of the two radars at the overlapped region. As Figs. 11 and 12 show, the major features of all three PRD match very well at the overlapped region (refer to overlapped region of two square boxes in Fig. 2). In addition, compared to background images (Figs. 3 and 4, the third row), Figs. 11 and 12 show more details. The detail is due to the fact that the X-band data have better range resolution and have contributed to the retrieval. The detailed part of the retrieval also has a good match for two radars. This fact convinces the validity of the variational retrieval algorithm introduced in this study.

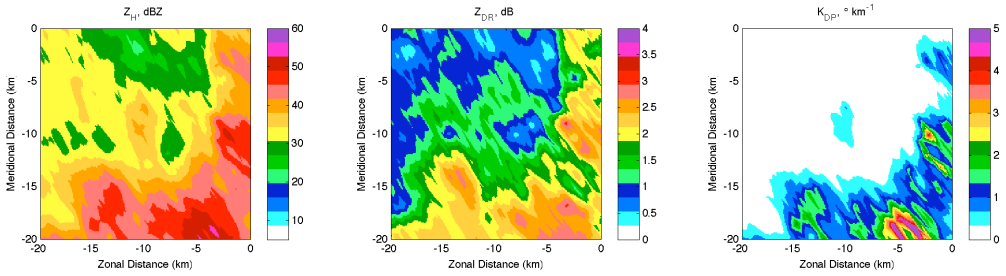

Fig. 11 Retrieved results based on KCYR radar measurements. The background was based on the retrieval of S-band radar (KOUN) measurements. From left to right: (a) Z_H, (b) Z_{DR}, (c) K_{DP}.

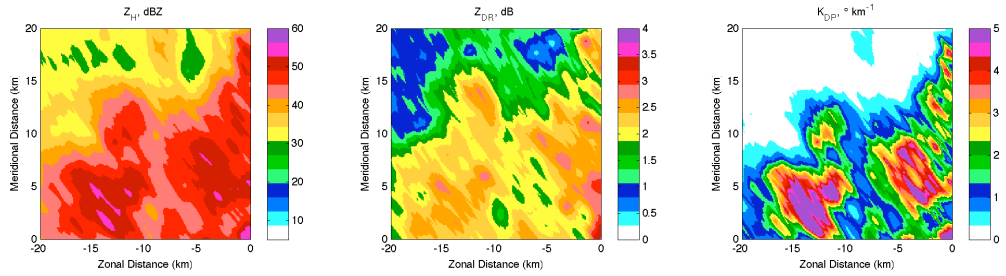

Fig. 12 The same as Fig. 11 but for the retrieval of KLWE radar measurement

5. DISCUSSIONS

The possible error sources for the variational retrieval algorithm may come from following factors.

The major source of the uncertainty comes from the data quality. According to the analysis of simulation and real data, the PRD of low SNR would deteriorate the retrieval remarkably if there were no useful information to correct them. At the region where the data quality is poor, the background is important. In this study, the background based on the S-band radar measurements has been applied to solve this problem. Nevertheless, The information used to aid the radar data quality can be provided from sources such as surface measurements, satellite measurements, model predictions, and so on.

The second one is the model error associated with the C-G DSD model. The variational algorithm treats the

two parameters of C-G DSD model as state variables. In reality, assumption of the C-G DSD may not be valid and is a possible source of error. However, our tests using data simulated using simpler exponential DSD suggests that the solution is not very sensitive to the DSD model assumed. The analysis of integral parameters (e.g., Z_H, Z_{DR}, and K_{DP}) is robust. The experiment using real data also implies this conclusion when X-band data quality is good or compensated by a reasonable background (e.g., S-band measurements).

The third source is the estimation of error spatial structure. The true magnitudes and correlations of the error covariance are never exactly known. In this algorithm, the spatial structure of background error covariance is modeled by a two-dimensional isotropic Gaussian function. The error magnitude of each PRD is set empirically. Our tests seem to show that the scales chosen in this study are appropriate.

Another source of error is the forward model. For the variational approach, observations and analysis fields are connected through the forward model. In this study, the forward model is based on the backscattering theory of raindrops. The radar might measure other species, such as snow and hail. When these species are presence in the radar sampling volumes, their effects have to be included in the forward model.

6. CONCLUSSIONS

This study proposed a variational retrieval algorithm based on attenuated radar measurements. The C-G DSD parameters were treated as the state variables in the variational scheme for the first time. Three PRD (Z_H, Z_{DR}, and K_{DP}) were optimized to correct the attenuation and do the retrieval by mitigating the effect of their measurement errors. The proposed lookup table method was demonstrated effective for the computation of complicated forward model and its partial derivatives. Preliminary results based on simulated and real PRD show the effectiveness of this variational algorithm.

In this case considered here, little or no hail existed at the low levels. When hail and/or other ice species are present, the problem will be more challenging. Additional constraint may be needed for successful retrievals.

ACKNOWLEDGEMENT

This work was supported by NSF grants ATM-0608168 and ATM-0530814. We appreciate Dr. Terry Schuur from NOAA National Severe Storms Laboratory (NSSL) who provided KOUN data, and Dr. Jerry Brotzge from CAPS who provided CASA IP1 data. We are also thankful for the helpful discussions with Dr. Jidong Gao, Dr. Ting Lei, and Gang Zhao.

Reference:

Berne, A., and R. Uijlenhoet, 2006: Quantitative analysis of X-band weather radar attenuation correction accuracy. *Nat. Hazards Earth Syst. Sci.*, **6**, 419–425

Brandes, E. A., G. Zhang, and J. Vivekanandan, 2004: Drop size distribution retrieval with polarimetric radar: model and application. *J. Appl. Meteor.,* **43**, 461-475

Bringi, V.N., T.D. Keenan, and V. Chandrasekar, 2001: Correcting C-band radar reflectivity and differential reflectivity data for rain attenuation: A self-consistent method with constraints. *IEEE Trans. Geosci. Remote Sens*., **39**, 1906–1915.

Bringi, V.N., V. Chandrasekar, N. Balakrishnan, and D. Zrnić, 1990: An Examination of Propagation Effects in Rainfall on Radar Measurements at Microwave Frequencies. *J. Atmos. Oceanic Technol.*, **7**, 829–840.

Cao, Q., G. Zhang, E. Brandes, T. Schuur, A. Ryzhkov, and K. Ikeda, 2008: Analysis of Video Disdrometer and Polarimetric Radar Data to Characterize Rain Microphysics in Oklahoma. *J. Appl. Meteor. Climatol.,* **47**, 2238–2255

Delrieu, G., H. Andrieu, and J.D. Creutin, 2000: Quantification of Path-Integrated Attenuation for X- and C-Band Weather Radar Systems Operating in Mediterranean Heavy Rainfall. *J. Appl. Meteor.*, **39**, 840–850.

Gao, J., M. Xue, K. Brewster, and K.K. Droegemeier, 2004: A Three-Dimensional Variational Data Analysis Method with Recursive Filter for Doppler Radars. *J. Atmos. Oceanic Technol.*, **21**, 457–469.

Gorgucci, E., and L. Baldini, 2007: Attenuation and Differential Attenuation Correction of C-Band Radar Observations Using a Fully Self-Consistent Methodology. *Geoscience and Remote Sensing Letters, IEEE*, **2**, 326-330

Hogan, R.J., 2007: A Variational Scheme for Retrieving Rainfall Rate and Hail Reflectivity Fraction from Polarization Radar. *J. Appl. Meteor. Climatol.*, **46**, 1544–1564.

Huang, X.Y., 2000: Variational Analysis Using Spatial Filters. *Mon. Wea. Rev.*, **128**, 2588–2600.

Ide, K., P. Courtier, M. Ghil, and A. Lorenc, 1997: Unified notation for data assimilation: Operational, sequential and variational. *J. Meteor. Soc. Japan*, **75,** 181-189.

Liu, H. and M. Xue, 2006: Retrieval of moisture from slant-path water vapor observations of a hypothetical GPS network using a three-dimensional variational scheme with anisotropic background error. *Mon. Wea. Rev.*, **134,** 933–949.

Liu, H., M. Xue, R. J. Purser, and D. F. Parrish, 2007: Retrieval of moisture from simulated GPS slant-path water vapor observations using 3DVAR with anisotropic recursive filters. *Mon. Wea. Rev.*, **135,** 1506–1521.

Liu, Y., V. Bringi, and M. Maki, 2006: Improved rain attenuation correction algorithms for radar reflectivity and differential reflectivity with adaptation to drop shape model variation. Proceedings. *IGARSS 2006*, Denver, Colorado

Meneghini, R., and L. Liao, 2007: On the Equivalence of Dual-Wavelength and Dual-Polarization Equations for Estimation of the Raindrop Size Distribution. *J. Atmos. Oceanic Technol.*, **24**, 806–820.

Park, S.G., V.N. Bringi, V. Chandrasekar, M. Maki, and K. Iwanami, 2005: Correction of Radar Reflectivity and Differential Reflectivity for Rain Attenuation at X Band. Part I: Theoretical and Empirical Basis. *J. Atmos. Oceanic Technol.*, **22**, 1621–1632.

Parrish, D. F. and J. C. Derber, 1992: The National Meteorological Center's spectral statistical-interpolation analysis system. *Mon. Wea. Rev.*, **120,** 1747-1763.

Ryzhkov, A., P. Zhang, D. Hudak, J. L. Alford, M. Knight and J.W. Conway, 2007: Validation of polarimetric methods for attenuation correction at C band. AMS, *33rd Conference on Radar Meteorology*, Cairns, Queensland, Australia, August 2007

Ryzhkov, A., and D. Zrnic, 1995: Precipitation and Attenuation Measurements at a 10-cm Wavelength. *J. Appl. Meteor.*, **34**, 2121–2134.

Testud, J., E. Le Bouar, E. Obligis, and M. Ali-Mehenni, 2000: The Rain Profiling Algorithm Applied to Polarimetric Weather Radar. *J. Atmos. Oceanic Technol.*, **17**, 332–356.

Vulpiani, G., F.S. Marzano, V. Chandrasekar, and S. Lim, 2005: Constrained Iterative Technique With Embedded Neural Network for Dual-Polarization Radar Correction of Rain Path Attenuation. *IEEE Trans. Geosci. Remote Sensing,* **43**, 2305-2314

Xue, M., M. Tong, and K. K. Droegemeier, 2006: An OSSE framework based on the ensemble square-root Kalman filter for evaluating impact of data from radar networks on thunderstorm analysis and forecast. *J. Atmos. Ocean Tech.*, **23,** 46–66.

Zhang, G., J. Vivekanandan, and M.K. Politovich, 2004: Radar/radiometer combination to retrieve cloud characteristics for icing detection. AMS, *11th Conference on Aviation, Range, and Aerospace.*, Hyannis, MA

Zhang, G., J. Vivekanandan, and E. Brandes, 2001: A method for estimating rain rate and drop size distribution from polarimetric radar. *IEEE Trans. Geosci. Remote Sensing,* **39**, 830-840.